Available online at www.sciencedirect.com
ScienceDirect
Journal of Photochemistry and Photobiology A: Chemistry 188 (2007) 298–310
Journal of Photochemistry and Photobiology A:Chemistry
www.elsevier.com/locate/jphotochem

Excited state intramolecular proton transfer (ESIPT) in a dioxotetraamine derived schiff base and its complexation with Fe(III) and Cr(III)

Suban K. Sahoo, Rati Kanta Bera, Minati Baral, B.K. Kanungo *

Department of Chemistry, Sant Longowal Institute of Engineering & Technology, Longowal 148106, India

Received 10 July 2006; received in revised form 9 November 2006; accepted 19 December 2006
Available online 27 December 2006

Abstract

The excited state intramolecular proton transfer (ESIPT) process in a symmetric Schiff base derived from dioxotetraamine and salicylaldehyde, *N*,*N*′-Bis{2-[(2-hydroxybenzylidine)amino]ethyl}malonamide (BHAEM) has been investigated experimentally by the fluorescent method and a two step proton transfer mechanism from dienol to ketoenol and then to diketo tautomer has been proposed on the basis of the theoretical evidence obtained through semi-empirical MO/CI calculations using the AM1 Hamiltonian. BHAEM on interaction with Fe(III) and Cr(III), in an aqueous medium of 0.1N ionic strength and 25 ± 1 °C forms monomeric metal complexes of the type ML and MLH_{-2} with both metal ions, whereas with Cr(III) it forms two more additional species, MLH and MLH_{-1}. The stabilities of these metal complexes have been evaluated using potentiometric and spectrophotometric methods and the relative stabilities of the complexes formed with this ligand are rationalized. At low pH, the ligand coordinates to the metal ions through bis-imine nitrogen and bis-phenolate oxygen atoms but with an increase of pH, further coordination occurs through two amide nitrogen atoms of the ionized amide groups. The structures of the metal complexes were predicted from minimum strain energy calculations employing molecular mechanics using the MM3 force field and from their theoretical electronic spectra obtained through semi-empirical AM1/ZINDO method.

Keywords: ESIPT; Schiff base; Potential energy surface (PES); Transition state search; Stability constants; Molecular mechanics; Semi-empirical method

1. Introduction

A burgeoning interest in Schiff bases derived from aromatic *ortho*-hydroxy aldehydes have recently attracted considerable attention owing to their importance to proteins [1], visual pigments [2], enzymic aldolization [3], decarboxylation reactions [4], pyridoxal phosphate degradation [5], color photography [6] and formation of metal complexes, which can be used as catalysts for the insertion of oxygen into organic substrates [7–11], clinical [12] and analytical fields [13]. Many such physical and biological properties of such Schiff bases are directly related to the presence of the intramolecular hydrogen bonds [14]. Though, in many *o*-hydroxy Schiff bases, both ground and/or excited state proton transfer (ESIPT) processes observed due to presence of intramolecular hydrogen bonding [15,16]; it is only during the last decade the excited state proton transfer has been subject of substantial interest [17–18]. In an ESIPT reaction, a fast enol-imine (E) to keto-enamine (K) prototopy occurs in the excited states of intramolecularly H-bonded molecules (Fig. 1). Such photo-physical processes led to potential applications involving the development of UV photo-stabilizers [19], molecular energy storage devices [20], dye lasers [21], high-energy radiation detectors [22] and fluorescent probes [23,24]. The majority of the studies on ESIPT processes to this date have been concentrated on the best-known photochromic Schiff base salicylidene aniline (SA) and related molecules [25–29]. The emission properties of these molecules have been shown to depend mainly on the solvent polarity, the pH, the hydrogen bonding character of solvent and the structures of the molecules [30–38]. Also, studies mostly by Maruyama and Inabe et al. [39] have been reported for the symmetric Schiff base derived from the aromatic diamine, *N*,*N*′-bis(salicylidene)-*p*-phenylenediamine (BSP). However, despite of the numerous reports on the photochromic behaviour of Schiff bases derived from aromatic amines, very little attention have been paid to the ESIPT emission of Schiff bases derived from aliphatic amine [40–42].

* Corresponding author. Tel.: +91 1672 284840; fax: +91 1672 284840.
E-mail address: b.kanungo@vsnl.com (B.K. Kanungo).

1010-6030/$ – see front matter © 2007 Elsevier B.V. All rights reserved.
doi:10.1016/j.jphotochem.2006.12.027

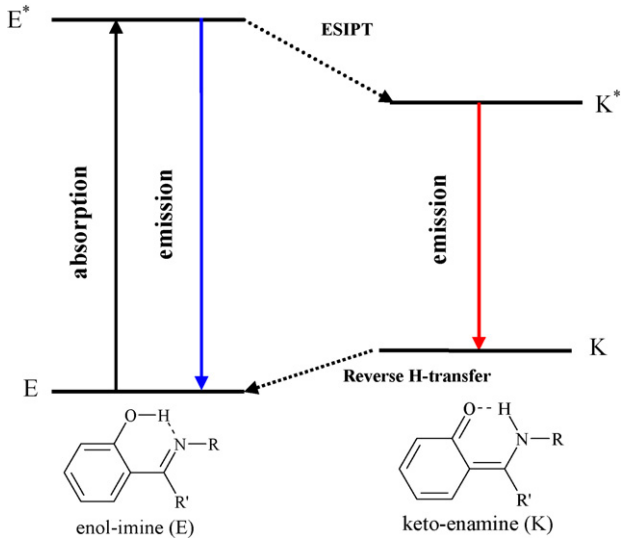

Fig. 1. Foster's cycle showing the excited state intramolecular proton transfer (ESIPT) from tautomer E^* to tautomer K^*.

Although there is a vast diversified research on Schiff bases now reported, the thermodynamic studies in solution carried out in order to obtain the protonation and stability constants of these kinds of compounds are scarce, due mainly to the insolubility in water of the neutral Schiff bases and their metal complexes and to the possible hydrolysis of these compounds in this medium leading to the starting organic fragments. Hence, thermodynamic studies of Schiff base complex formation in solution have been carried out in organic or mixed aqua-organic solvents in which the ligand and its complexes are soluble [43–45]. Only few examples of such studies in pure aqueous medium are known [46]. In an earlier study, we have shown that the Schiff base *N*,*N*′-Bis{2-[(2-hydroxybenzylidine)amino]ethyl}malonamide (BHAEM), which contains two amide, imine and phenolate groups in aqueous solution is quite stable below pH ∼ 8 and has shown peculiar coordination behaviour [47]. BHAEM, in acidic condition, coordinates through two imine nitrogen atoms and two phenolate oxygen atoms with Co(II), Ni(II), Cu(II) and Zn(II), whereas in slightly acidic and basic condition, the two amide groups coordinate only to Cu(II) and Ni(II) but not to Co(II) and Zn(II) [47].

Keeping in view the importance of Schiff bases and their pronounced phototropic and photochromic properties along with the interesting coordination behaviour of BHAEM, we continued to focus our attention on the symmetric Schiff base and specially on the proton transfer and its interaction with the trivalent metal ions, Fe(III) and Cr(III). The present work describes the ESIPT reaction that occurs for *N*,*N*′-Bis{2-[(2-hydroxybenzylidine)amino]ethyl}malonamide (BHAEM) with respect to the concentration, excitation wavelength and pH using the fluorescent method. The complexation behaviour of BHAEM with Fe(III) and Cr(III) is evaluated through potentiometric and spectrophotometric methods in aqueous medium and the stability constants of the complexes are obtained. Molecular modeling calculations are carried out using both empirical and semi-empirical methods in order to explain the experimental behaviour.

2. Experimental

2.1. Materials and measurements

The Schiff base, *N*,*N*′-Bis{2-[(2-hydroxybenzylidine)-amino]ethyl}malonamide (BHAEM) was synthesized as reported [47]. All solvents were purchased from Merck and used as received. All the solutions employed for the fluorescent study were prepared by dilution from a stock solution of BHAEM (10^{-3} M). The final concentration of BHAEM was maintained at ∼1 to 2×10^{-5} M and the fluorescence spectra were recorded on a Perkin-Elmer LS55 luminescence spectrometer. The electronic spectra were recorded on an Agilent-8453 diode array UV-VIS spectrophotometer.

2.2. Titration procedure

All solutions for potentiometric study were prepared from doubly distilled water. Metal ion solutions of 0.01 M were prepared from reagent grade chloride salts of iron and chromium obtained from Merck. Carbonate free 0.1 M KOH solution was prepared and standardized against potassium hydrogen phthalate. A stock solution of the ligand (0.01 M) was prepared by dissolving an appropriate amount in calculated quantity of 0.1 M HCl solution (standardized against standard KOH) to make the former water-soluble by converting it into its chloride salt. 1 M KCl solution was used as electrolyte.

In the potentiometric titrations, the observed pH was measured as $-\log[H^+]$ using a Thermo Orion 720A$^+$ pH meter equipped with a combined glass electrode calibrated with standard buffer solutions [55]. The potentiometric titrations were carried out at 25 ± 1 °C maintained from a double wall glass jacketed titration cell connected to a constant temperature circulatory bath. The ionic strength was maintained to 0.1 M KCl with the addition of appropriate amount of 1 M KCl solution. The titrations were carried out over the pH range of 2.5–11.0 and sufficient time was given for the attainment of equilibrium to yield a stable pH reading and each experiment was repeated three times. The final concentrations of 10^{-3} M ligand and 10^{-3} M metal ion solution were maintained for all titrations. The equilibrium constants obtained from potentiometry were calculated using the computer program Hyperquad-2000 [56], ($pK_w = 13.78 \pm 0.05$).

The stability constants of the complexes were also determined spectrophotometrically in aqueous medium. The procedure used for the potentiometric and spectrophotometric titrations was similar; a dilute solution of ligand (1.26×10^{-4} M) with HCl (1.26×10^{-3} M) was titrated with 0.1 M KOH at an ionic strength of 0.1 M KCl and 25 ± 1 °C in aqueous medium. After each adjustment of pH, an aliquot was removed and the electronic spectra was recorded. The protonation constants from the spectral data were calculated using a non-linear least-square fitting program, pHAb [57].

2.3. Computational methods

All calculations were carried out on a Pentium IV 3.0 GHz machine with Windows 2000 environment. The ground state geometry of BHAEM leading to minimum strain energy was achieved through molecular mechanics using the MM3 force field followed by semi-empirical AM1 self-consistent fields (SCF) method, at the Restricted Hartree-Fock (RHF) level with a convergence limit of 0.0001 kcal/mol and an RMS gradient of 0.001 kcal/mol. The geometry of BHAEM in the excited state was calculated using the AM1 Hamiltonian by taking into account the configuration interaction (CISD = 4 in MOPAC with total configuration 1000). The electronic spectrum of BHAEM was calculated by applying the semi-empirical AM1/ZINDO method.

The transition state structures of BHAEM during intramolecular proton transfer reaction in the ground state were calculated using HyperChem version 7.5 [58]. The initial optimized geometries (reactants and products) obtained from MM calculation were re-optimized using the semi-empirical AM1 method and taken further to calculate the possible transition state geometries. The algorithm as reported by Peng and Schlegel, i.e., a synchronous transit state method with quadratic interpolation between the reactants and products states was used [59]. The starting structures for the transition state search were obtained by merging both minimized reactant and product in the workspace through the reaction map option in the program. Each refined transition state geometry was then verified from the presence of a negative frequency in the vibrational spectrum.

The initial 3-D structure related to the probable geometry of each metal complex was obtained through the comprehensive option of the computer program, CAChe version 6.1.1 [60] and the related minimum strain energy was calculated. For both Fe(III) and Cr(III) all possible six coordinated structures were examined. The geometries of the complexes were energetically optimized through molecular mechanics applying the MM3 force field in *vacuo* with the Polka-Ribiere algorithm and RMS gradient 0.001 kcal/mol. Further, the least strain energy structures were re-optimized using the semi-empirical AM1/d method and the electronic spectra were calculated using the semi-empirical ZINDO method.

3. Results and discussion

3.1. Absorption spectra and ground state structure

The absorption spectrum of BHAEM in ethanol, acetonitrile and dimethylsulfoxide shows three peaks at ∼213, ∼255 and ∼317 nm. The first and the second peaks were attributed to $\pi \rightarrow \pi^*$ transitions associated with the phenyl ring and the azomethine chromophore, respectively, whereas the third peak was assigned to the $n \rightarrow \pi^*$ transition from the imine nitrogen atom in conjugation with the phenol group. The later band within the region 300–350 nm is generally assigned to the intramolecular hydrogen bonded enol isomer. The presence of an intramolecular H-bond can also be assigned from the ^{1}H NMR spectrum of BHAEM. The phenolic proton peak of BHAEM was appeared at 13.1 ppm in $CDCl_3$ [47]. Such downfield shifting of the OH group is due to a decrease in the electron density around the OH proton upon strong intramolecular hydrogen bonding. Similar downfield chemical shifting was also reported for salicylidene methylamine (13.50 ppm, $CDCl_3$) assigned to the closed enolic conformer [16]. When the intramolecular bonding is not involved, or is very weak, the enolic protons usually absorb in the same region as the phenolic protons. The *o*-hydroxy Schiff bases having intramolecular H-bonds generally undergo tautomerization from enol-to-keto and/or keto-to-enol. Such a tautomerization process from enol-to-keto in Schiff bases is a common phenomenon in solution, which ruptures the aromaticity by decreasing the number of delocalized electrons in the phenyl ring from six to four. This process is favorable for Schiff bases derived from *o*-hydroxy naphthaldehyde or any other aldehydes having conjugated aromatic systems because the rupture in aromaticity of one phenyl ring is compensated by the presence of the other aromatic rings [16]. However, such a process is less favorable in Schiff bases derived from salicylaldehyde, as is the case for BHAEM. Moreover, the calculated heat of formation obtained through the semi-empirical PM3 method [47] and in the present study using the AM1 Hamiltonian (Table 1), indicate that the most stable enol form of BHAEM occurs in the ground state.

The absorption spectra of BHAEM in ethanol, acetonitrile and dimethylsulfoxide were recorded on successive addition of acid. The recorded absorption spectra of BHAEM in ethanol upon step-wise addition of acid (10^{-3} M HCl in ethanol) are shown in Fig. 2a. The peaks at 255 and 317 nm shifted to higher wavelength 278 and 346 nm, respectively, whereas the peak at 213 nm shifted hypochromically and the yellow color disappeared completely as C_{acid}:$C_{BHAEM} \geq 2$. Similar changes were observed in the other medium also. In a previous study, the absorption spectra of BHAEM in aqueous medium on successive increase in the pH showed bathochromic shifts due to the deprotonation of phenolic groups to form phenolate ions, where the non-bonding electrons in the anion are available for interaction with the π-electron system of the benzene ring [47]. Contrary to this observation, the shifting of the BHAEM (considered as LH_2) peaks in polar organic solvents upon successive addition of

Table 1
Heat of formation (H_f, kcal/mol), total energy (E_T, eV) and electronic properties of BHAEM calculated through semi-empirical AM1 method[a]

Parameters	Dienol	Ketoenol	Diketo	TS1	TS2	TS3
ΔH_f	−76.41 (−4.30)	−73.47 (−36.10)	−68.94 (−29.02)	−54.18	−49.54	−49.64
E_T	−5127.77 (−4677.37)	−5127.64 (−4678.75)	−5127.44 (−4678.45)	−5583.55	−5578.92	−5579.01
S_0–S_1 (absorption)	208, 248 and 286 nm	–	–	–	–	–
S_1–S_0 (emission)	313.5 nm	–	568.6 nm	–	–	–

[a] Values in parenthesis are for the excited singlet state geometry of BHAEM.

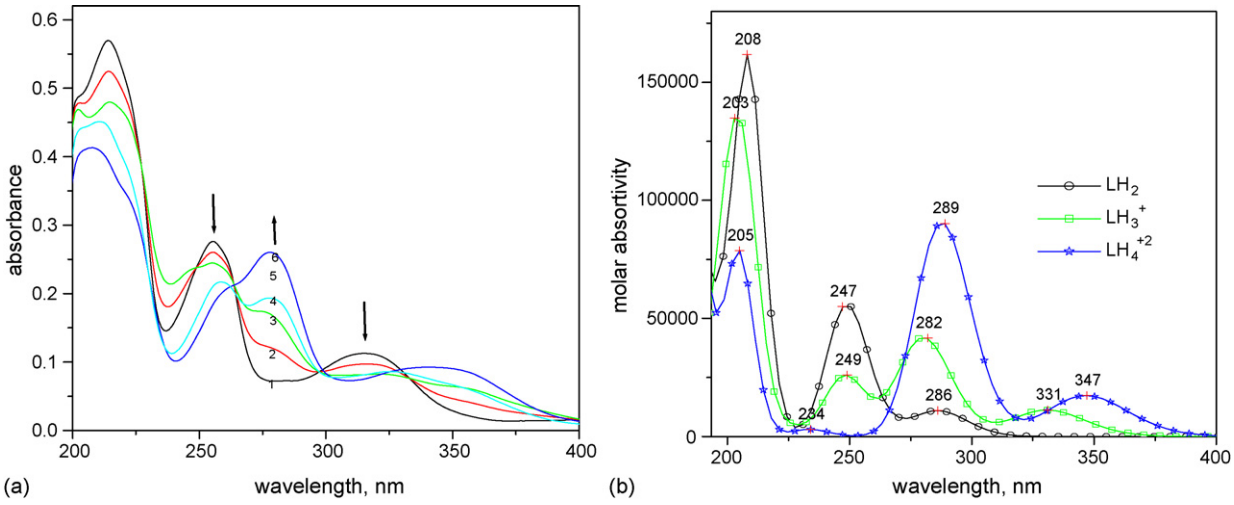

Fig. 2. Electronic spectra of (a) 10^{-5} M BHAEM on the successive addition of 10^{-3} M HCl and (b) three species (LH_2, LH_3^+ and LH_4^{2+}) of BHAEM calculated using the semi-empirical ZINDO method.

HCl towards higher wavelength may be due to the protonation of imine nitrogens, which results in a breaking of the intramolecular O–H···N H-bond. This process leads to the formation of new protonated species LH_3^+ and LH_4^{2+}. The breaking of H-bonds may result in an enhancement in the π-electrons delocalization upon interaction of unpaired electrons from the auxochrome hydroxyl groups, which is initially transferred toward hydrogen atom bonded intramolecularly to the imine group.

Molecular modeling calculations were carried out using the semi-empirical AM1 method in *vacuo* for the different possible conformers of LH_3^+ and LH_4^{2+}. Based on the calculations, it was found that protonated BHAEM favours a *cis*-form in which the proton attached to the imine nitrogen atom linked intramolecularly to the oxygen atom (Fig. 3(A)b). The electronic spectra of the minimized structure BHAEM (LH_2), calculated applying the semi-empirical ZINDO method (Fig. 2b), shows three peaks with λ_{max} at 208, 247 and 286 nm. The peak at 208 nm shifted hypochromically whereas the remaining two peaks (247 and 286 nm) shifted to higher wavelength (282 and 331 nm) and (289 and 347 nm) for the species LH_3^+ and LH_4^{2+}, respectively, with concomitant rise in the molar absorptivity. This corroborates well with the experimental results (Fig. 2a). The HOMOs with λ_{max} at 286 and 347 nm for the species LH_2 and LH_4^{2+}, respectively, are shown in Fig. 3(B). It was observed that, in closed enolic form (LH_2), the electronic contribution by the auxochrome hydroxyl groups was distributed to both the aromatic and imine groups, whereas the rupture of the O–H···N bond due to the protonation of imine nitrogen atoms increases the electron delocalization from the hydroxyl group towards the aromatic system which is in conjugation with the imine linkage and this decreases the energy gap between the HOMOs and LUMOs.

3.2. Emission spectra and excited state structure

The fluorescence emission measurements of BHAEM were made at room temperature in different solvents: water, ethanol, acetonitrile and dimethylsulfoxide (DMSO) and also at varying concentration, excitation wavelength and pH. The emission spectra of BHAEM on excitation at 317 nm shows two bands: (i) one weak band at ∼350 nm in all the above organic solvents but not in aqueous medium where it was observed at 367 nm and (ii) another broad band between ∼410 and 430 nm. The weak emission band found to be prominent in proton donor solvents water and ethanol, but slightly broaden in DMSO and acetonitrile. Appearance of such discrepancy is due to the ability by the proton donor solvents to form intermolecular hydrogen bonds with the nitrogen atoms of BHAEM. The first weak emission band can be assigned to the direct emission from the intramolecularly H-bonded enol form, whereas the emission band with higher intensity can be assigned to the de-excitation from the keto form of BHAEM that is formed in the excited state by tautomerization. Such prototropic behaviour of Schiff bases in the excited state is expected because at this state the intramolecularly hydrogen bonded acidic (proton donor) and basic (proton acceptor) groups become more acidic and basic, respectively. This causes an easy path for proton transfer from the acidic to basic group, and generates new keto tautomer, which emits at lower energy/higher wavelength. By performing fluorescence spectroscopic studies of 3-hydroxy-1-*p*-carboxyphenyltriazene (HT) Ressalan and Iyer proposed that at the excited state the enol form rearrange into keto form by proton transfer with the formation of equilibrium between enol and keto species, which results de-excitation of weak and broad bands at shorter and longer wavelength, respectively [61]. Hence, the peak obtained at higher wavelength is assigned to the keto form of BHAEM.

The excitation spectrum of BHAEM, obtained on monitoring the 405 nm emission, showed two bands at 267 and 346 nm, which is similar to its absorption spectrum. The emission spectra taken in ethanol at different concentrations, when excited at 317 nm are shown in Fig. 4a. A variation in the spectra was observed between 2.5×10^{-5} and 0.035×10^{-5} M. The spectra showed two isosbestic points at 367 and 406 nm. The broad band (assigned to the keto form) became sharper on dilution and shifted towards higher wavelength, whereas the weak band (assigned to the enol form) was independent of concen-

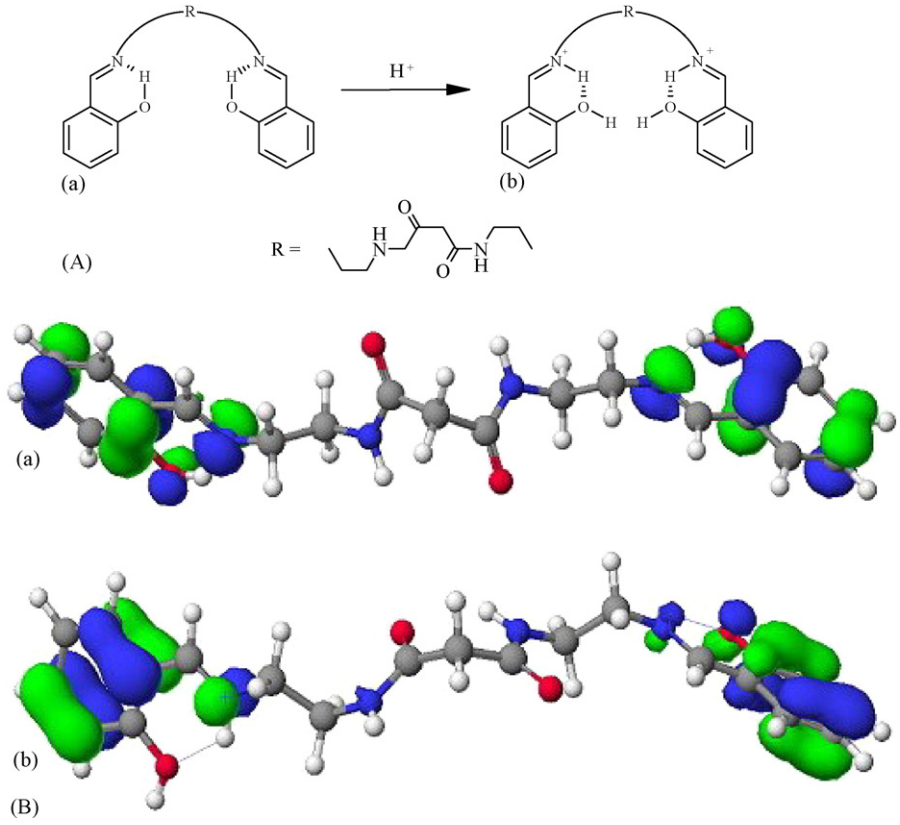

Fig. 3. (A) The neutral LH_2 (a) and fully protonated form LH_4^{2+} (b) of BHAEM showing intramolecular H-bonding; (B) the HOMO diagrams corresponding to the peak at λ_{max} at (a) 286 nm for LH_2 and (b) 347 nm for LH_4^{2+} calculated (by the semi-empirical AM1/ZINDO method) for BHAEM.

tration, but its intensity increased slightly with dilution. These observations thus indicate that ESIPT process in BHAEM is concentration dependent. Also, the emission bands of BHAEM were recorded with respect to the change in excitation wavelength (λ_{exc} = 317–335 nm) at 10^{-5} M in all the above solvents. The λ_{exc} dependent spectra of BHAEM taken in DMSO are shown in Fig. 4b. It was observed that with increase of the excitation wavelength the weak band due to the enol form disappeared while an increase in the intensity of the emission band of the keto form was noticed. These observations infer a complete conversion of the enol form to the keto tautomer due to increase of the excitation wavelength.

The changes in the fluorescence spectrum of BHAEM with respect to pH in aqueous medium, when excited at 330 nm are shown in Fig. 5. The spectra show that between pH 3.88 and 7.32, no change in the emission band is observed (Fig. 5a). As the pH

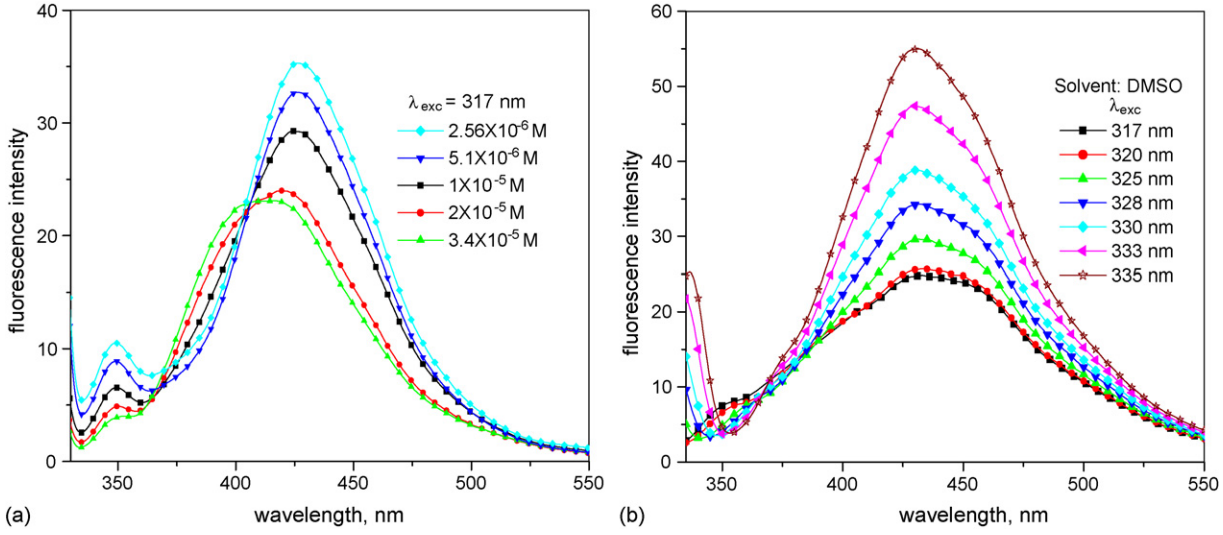

Fig. 4. The emission spectra of BHAEM at (a) different concentrations in ethanol and (b) different excitation wavelength in DMSO.

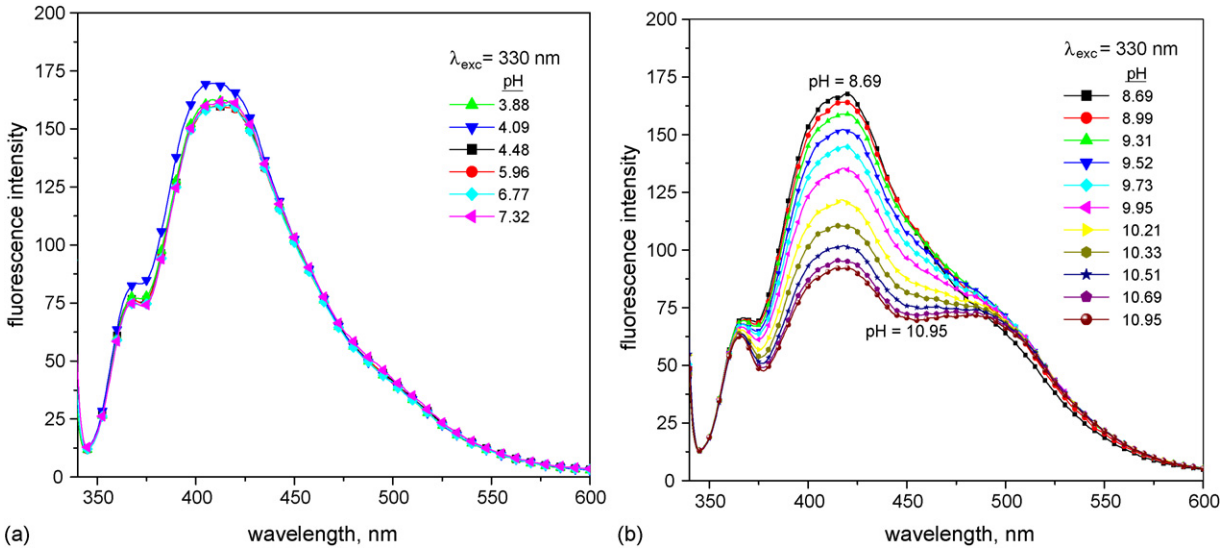

Fig. 5. Emission spectra of BHAEM at different pH values in water.

raises further, the intensity of the band (at ∼425 nm) decreases whereas the intensity of other band increases; Also a new peak appears at ∼500 nm. This clearly indicates that BHAEM produces different species in the excited state with respect to the change in pH. At low pH, both enol and keto form of BHAEM are the dominant species in solution. However, the relative formation of keto species decreases with the increase in pH, which can be attributed from the decrease in intensity of the band at ∼425 nm. In more basic medium, BHAEM is susceptible to hydrolysis which can be shown from the appearance of new band at ∼500 nm, where the free salicylaldehyde gave characteristic emission band due to ESIPT process [62]. The mechanism for the hydrolysis of BHAEM in basic conditions has already been explained [47] where the hydroxyl ion attacks the imine nitrogen atom and subsequent rearrangement results in breakage of the imine linkage and then leads to the back formation of aldehyde and amine.

3.3. Molecular modeling calculations

In order to get more insight into the tautomerization process in the excited state, semi-empirical AM1 calculations were performed. This method is claimed to describe the energetics and topographies of hydrogen bonded systems fairly accurately and also provides good estimates of geometries and heats of formation of organic molecules in the excited state [63]. Some calculated physical parameters of BHAEM are given in Table 1. In contrast to the ground S_0 state, it was found that the keto form of BHAEM is energetically more stable than its enol form at the first excited singlet state. Further, the calculated S_1–S_0 electronic transition (emission spectrum) for the enol and keto forms of BHAEM was obtained at 313 and 569 nm, respectively, which agree well with the experimental observations.

3.3.1. Transition state structures

BHAEM is a symmetric di-Schiff base that has two equivalent intramolecular proton transfer reaction site and may exist in three tautomeric forms: two symmetric structures, “dienol” and “diketo”, and one non-symmetric, “ketoenol”. The ground and excited state geometries of these three possible tautomeric forms of BHAEM have been calculated. The calculated different physico-chemical parameters are given in Table 1.

The ΔH_f data predicts the dienol tautomer in the ground state whereas in the excited singlet state ketoenol and diketo tautomers are more stable. Further, in the excited state the higher stability of the keto–enol form than the diketo form suggests that, in the excited state an intermediate species ‘ketoenol’ can form before it converted into diketo form. The tautomerization energy in the ground state is 7.59 kcal/mol and indicates that the intramolecular proton transfer process is endothermic whereas in excited state, it is exothermic in nature (−24 kcal/mol).

Considering the fact that the intermediate ‘ketoenol’ species is more stable in excited state, transition state structures were evaluated using the AM1 Hamiltonian for the ground state only to propose the possible routes for the proton transfer during tautomerization. Two possible routes for tautomerization of BHAEM were considered: (i) an asynchronous proton transfer was considered in which the proton transfer from the dienol species to the tautomer ketoenol (as intermediate structure, TS1) followed by a transference of a second proton and the diketo tautomer is formed (TS2), (ii) one step synchronous proton transfer from the dienol to the diketo tautomer (TS3) is considered. The calculated transition state structures of BHAEM (TS1, TS2 and TS3) are shown in Fig. 6 and their physical parameters are given in Table 1. The transition state structures were also verified from the calculated infrared frequencies. It is known that if the geometry obtained from an optimization run corresponds to the global minimum all the frequencies are real and positive. But, if the geometry at transition state or any stationary point is other than a minimum, some of the frequencies will be complex and result negative values, which are often called “imaginary frequencies”. A well-behaved transition state structure for a reaction will have one imaginary frequency. In the present study the calculated transition state structures were verified from imaginary frequen-

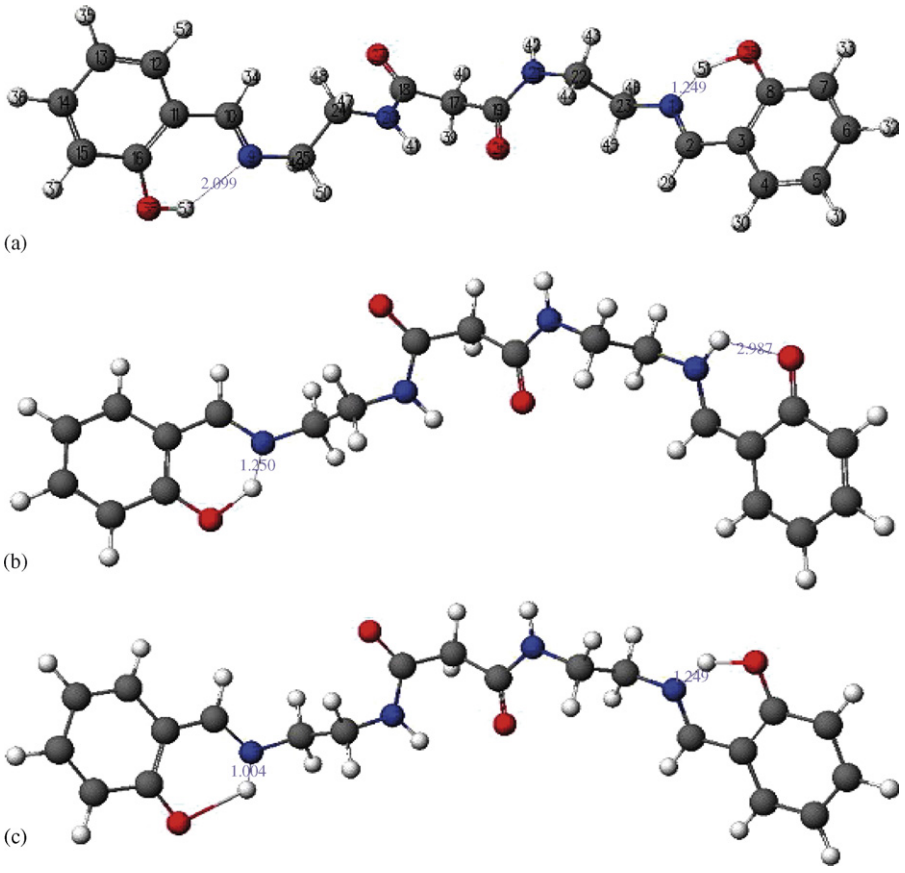

Fig. 6. Transition state structures corresponding to the tautomerization processes (a) Dienol → Ketoenol (TS1), (b) Ketoenol → Diketo (TS2) and (c) Dienol → Diketo (TS3) in BHAEM calculated by the AM1 method.

cies at −2065.3i, −2063.9i and −2067.5i for TS1, TS2 and TS3, respectively.

Table 1 reveals that the calculated barrier height for the reaction which occurs by a synchronous mechanism (TS3), is higher than the calculated barriers for the asynchronous mechanism (TS1 or TS2). For the calculated transition state (TS3) during the dienol → diketo prototropic reaction, it was found that the N···O distance (N(1)–O(28) = 2.465 Å and N(9)–O(38) = 2.787 Å) through which the proton is transferred was found to be shortened more in one reaction site compared to the other. Again, the weak hydrogen bond in the S_0 state for the dienol system (H···N ≈ 2.101 Å) upon tautomerization in transition state (TS3) forms fairly stronger two dissimilar H···N bonds (bond length 1.249 and 1.004 Å) at the two reaction sites (Table 1). Considering all aforesaid observations, it can be suggested that the proton migration during tautomerization in one reaction site is much faster than for the other reaction site, and that is why the asynchronous reaction mechanism is be preferred.

3.3.2. Potential energy surface (PES)

Since the relative tautomer energies differ in the ground and the excited electronic states, it is pertinent to examine the activation barriers to the proton transfers in both these states. To construct the reaction path representing the proton transfer in BHAEM, the N(1)–H(51) and N(9)–H(53) distance was chosen as the co-ordinate. The potential energy surface (PES) for the proton transfer reaction was generated through the calculation of the energies of the configurations with varying N(1)–H(51) and N(9)–H(53) distance, one at a time, as well as simultaneously. At each point, all other geometrical parameters were optimized and the calculated PES curves are shown in Fig. 7.

The maxima in the S_0 state is a true saddle point on the potential energy surface and occurs at a proton transfer distance

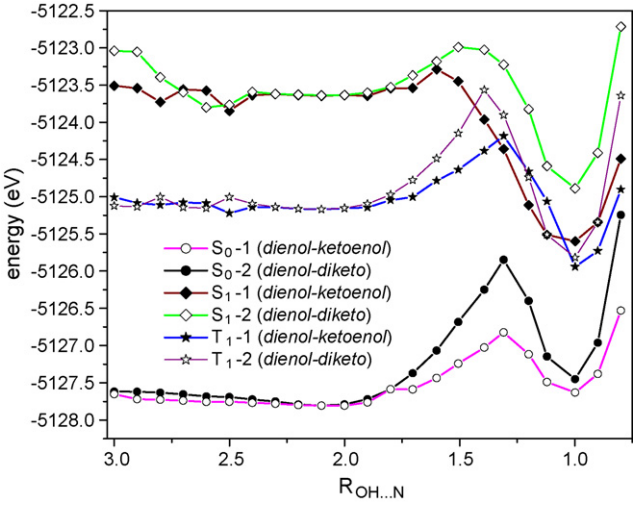

Fig. 7. Potential energy profiles for intramolecular proton transfer in both states.

of 1.3 Å. It turns out that the reaction is appreciably endothermic in the S_0 state and the activation energy for the transfer is also quite high. Thus, proton transfer in the S_0 state is unlikely to occur. On the other hand, the tautomeric form in the excited state (S_1) is predicted to be relatively more stable than the primary closed form. The barrier height for proton transfer is smallest for the S_1 state and the process is predicted to become an exothermic one. The barrier height is relatively low both in the S_1 and T_1 states compared to the S_0 state. Thus, proton transfer is possible in the excited states, which agrees well with the experimental results. Again, from the PES diagram in all three states, it was also observed that the barrier height for the single proton transfer is predicted to be more favorable than the simultaneous double proton transfer.

3.4. Metal complexes

The determination of formation constants for BHAEM (H_2L) with Fe(III) and Cr(III) was carried out by both potentiometric and spectrophotometric methods. Metal–ligand molar ratios 1:1 and 1:2, ionic strength $\mu = 0.1$ M KCl and temperature 25 ± 1 °C were maintained for the potentiometric titration in aqueous medium. The titration curves for the 1:1 metal–ligand molar ratio for all the metal ions along with the free ligand are shown in Fig. 8, where symbols represent the data collected when no turbidity or solid phase appeared, and dashed lines represent points collected when the solution turned turbid or precipitate appeared. The deviations in the metal–ligand titration curves from the titration curve for the ligand alone implied the formation of metal complexes. The formation of precipitate was observed between pH ≈ 8 and 9 in both cases and this data (dashed lines) were not used for calculation. The cause of precipitation of the metal complexes may be due to their insolubility in aqueous medium at higher pH and/or more likely due to the hydrolysis of the ligand and its metal complexes. Analyses of

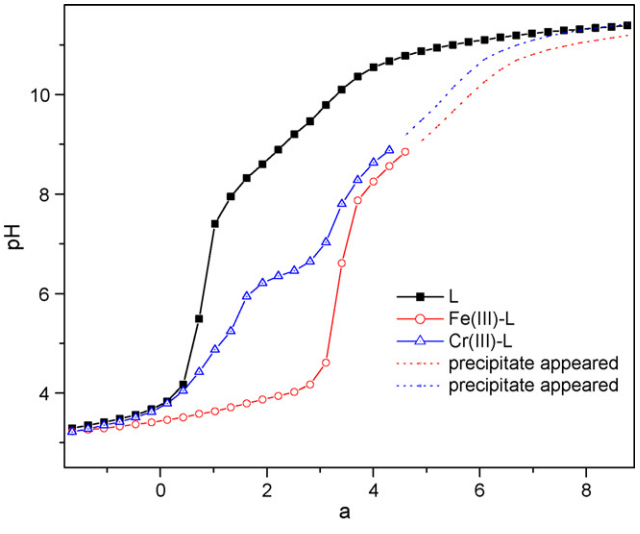

Fig. 8. Potentiometric titration curves for BHAEM in the absence and presence of metal ions: Fe(III) and Cr(III) in 1:1 ligand-metal molar ratio, where '*a*' is moles of base added per mole of ligand present (symbols indicate the experimental values, whereas dotted lines indicate the appearance of precipitation).

Table 2
Protonation [47] and formation constants (log β) of BHAEM at 25 ± 1 °C and $\mu = 0.1$ M KCl (**A**, potentiometry and **B**, spectrophotometry)

Equilibrium	log β	
	A	**B**
$L + H \rightleftharpoons LH$	8.20 ± 0.03	8.12 ± 0.01
$L + 2H \rightleftharpoons LH_2$	15.65 ± 0.03	15.32 ± 0.01
$Cr + L + H \rightleftharpoons CrLH$	14.33 ± 0.07	14.25 ± 0.05
$Cr + L \rightleftharpoons CrL$	8.33 ± 0.04	8.31 ± 0.02
$Cr + L \rightleftharpoons CrLH_{-1} + H$	1.86 ± 0.03	1.69 ± 0.02
$Cr + L \rightleftharpoons CrLH_{-2} + 2H$	−5.31 ± 0.02	−5.20 ± 0.04
$Fe + L \rightleftharpoons FeL$	10.93 ± 0.09	10.85 ± 0.02
$Fe + L \rightleftharpoons FeLH_{-2} + 2H$	3.68 ± 0.01	3.90 ± 0.05

the potentiometric curves by Hyperquad 2000 allowed the determination of various metal complex species in equilibrium and their formation constants are summarized in Table 2. The best fit models included MLH, ML, MLH_{-1} and MLH_{-2} for Cr(III) whereas only two species ML and MLH_{-2} were obtained for Fe(III). Measurements were also made on solutions containing a metal to ligand ratio 2:1, but no binuclear species were detected. One of the most important drawbacks while investigating the thermodynamic parameters of Schiff bases in water is the pH dependent hydrolysis of imine linkage. In the present case, when the expected hydrolysis products were incorporated in the model during calculation, the fit was worsened or rejected during the refinement process. The stability of BHAEM in acidic medium [47] has already been reported. Again, as evident from the result, the complexes formed in acidic medium also resist the hydrolysis of imine linkage at low pH range. The formation of the various species from the best-fit model can be represented by the following equations:

$$M + L + H \rightleftharpoons MLH, \quad \log \beta_{MLH} = \frac{[MLH]}{[M][L][H]} \tag{1}$$

$$M + L \rightleftharpoons ML, \quad \log \beta_{ML} = \frac{[ML]}{[M][L]} \tag{2}$$

$$M + L \rightleftharpoons MLH_{-1} + H^+, \quad \log \beta_{MLH_{-1}} = \frac{[MLH_{-1}][H^+]}{[M][L]} \tag{3}$$

$$M + L \rightleftharpoons MLH_{-2} + 2H^+, \quad \log \beta_{MLH_{-2}} = \frac{[MLH_{-2}][H^+]^2}{[M][L]} \tag{4}$$

The interaction of Fe(III) and Cr(III) with BHAEM (L) was also studied by the spectrophotometric method to probe the different possible coordination modes of BHAEM in solution. Spectrometric titrations of BHAEM were carried out in 1:1 metal-to-ligand ratios with the ligand concentration $[L] = 1.26 \times 10^{-4}$ M and the metal ion concentrations $[M(III)] = 1.26 \times 10^{-4}$ M with increasing pH between ~3.5 and 9.0. No spectral changes were observed at pH values below ~3.5 and plots for this region are excluded. Above pH ~9.0, the solution became turbid. The experimental electronic spectra

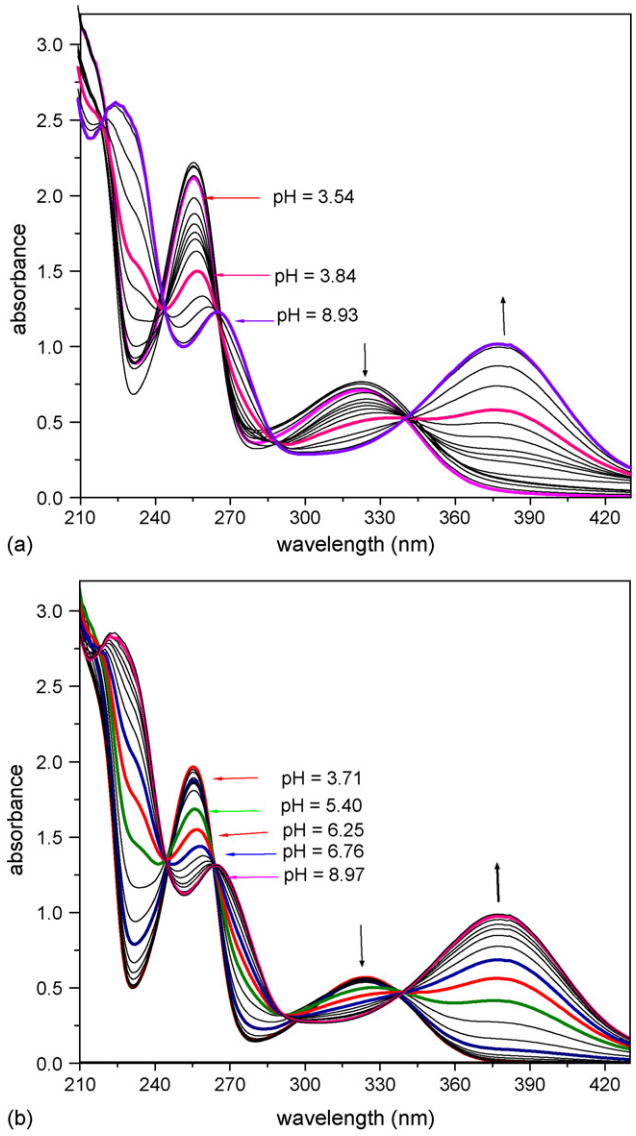

Fig. 9. Experimental electronic spectra for 1: 1 metal to BHAEM ratio with (a) Fe(III) and (b) Cr(III) with increasing pH.

for the BHAEM-M(III) systems are given in Fig. 9. Major spectral changes were observed between pH ∼3.5 and 9.0, which is in accord with metal complexation occurring. The variations in electronic spectra for both the metal ions at different pH are quite similar and suggest a similar mode of complexation. The ligand peaks at 255 and 324 nm at the initial pH were shifted towards higher wavelengths 267 and 378 nm, respectively; with concomitant rise in the absorbance. The shifting of peaks was reflected by the formation of isosbestic points**.** No additional band specific to the chelate(s) appeared at long wavelengths. The best-fit model was obtained when formation of the species ML and MLH_{-2} in case Fe(III) system and MLH, ML, MLH_{-1} and MLH_{-2} in case Cr(III) system were considered. The formation constants were calculated from the spectral data using the computer program pHAb and the values are given in Table 2.

The solution species distribution curves (Fig. 10) indicate that complexation occurs from pH ∼ 3. BHAEM, which initially exists in its fully protonated form LH_2 starts to deprotonate and lead to the formation of MLH and ML species with maximum percentage occurring at pH 5.3 and 6.0, respectively, in the case of the Cr(III) system, whereas the ML species in the case of the Fe(III) system exits with maximum percentage at pH 3.7. Stochiometrically the two moles of proton are released from the free ligand within this pH region can be clearly assigned to the participation of the phenolic group in metal complexation (the protonation constants have been determined). Again, the ligand peaks (Fig. 9) shifted bathochromically upon on increase in pH from ∼3.5 and this is also attributed to the deprotonation and coordination of the chromophoric unit phenol as phenolate ion. This results in stabilization of the π^* excited state due to charge delocalization and brings the lowest excited state closer to the highest ground state and thus results in a lower energy (longer wavelength) for transition. Thus, formation of the ML species is proposed to result from the coordination of the fully deprotonated ligand via its two imine nitrogen atoms and two phenolate oxygen atoms whereas in the case of the monoprotonated species MLH the metal is tricoordinated by the ligand, with one of the phenol oxygen atoms remaining protonated. It has been well established that $CrCl_3$ and $FeCl_3$ exist as hexacoordinated $[Cr(H_2O)_6]^{3+}$ and $[Fe(H_2O)_6]^{3+}$ in aqueous solution [64]; thus it is expected that in MLH and ML species three and two water molecules, respectively, will coordinate to fulfill the required coordination number. Three different possible coordination modes can be proposed for ML, two of which correspond to $ML(H_2O)_2$ with the water molecules in *cis* and *trans* positions (Fig. 11). It has been reported in the literature that the relative flexibility of (N,O-donor) tetradentate Schiff base ligands of the present type allows formation of metal complexes with an 'umbrella' or 'stepped' shaped geometry for which two water molecules are able to coordinate in *cis* positions [65]. Accordingly, structures **A** or **C** are expected to predominate over **B**. Again, the stability constant of the species, FeL, is seven log unit lower than that reported for Fe(salen) in DMSO–water 80:20 wt/wt medium [43]. Such a difference may be due to the difference in the medium but also to the formation of a 12-membered ring, which is expected to contribute to lower stability.

As the pH increases, formation of $CrLH_{-1}$, $CrLH_{-2}$ and $FeLH_{-2}$ were observed and the species, MLH_{-2} (M = Cr(III) and Fe(III)) was predominant at higher pH values (Fig. 10). The loss of protons from the complex ML may result either from the coordinated water molecules or through the ionization of the amide groups. In the present case, a bathochromic spectral shift with increase in pH (Fig. 9) indicates further participation of the ligand's architecture in coordination, and suggests that it is coordinated through anionic amide nitrogen atoms rather than reflecting deprotonation of the coordinated water molecules. It is well-known that anionic amide groups coordinate are able to form strong bonds with transition metal ions in higher oxidation states [66]. Such complexation may be proposed for both the present trivalent metal ions. It has been shown that in a ligand bearing a bis-amide and bis-amino framework, the dioxo oxygen atoms do not participate in the complex formation [53,54]. Considering the above evidence, three different hexadentate configurations (Fig. 11) are proposed for the species MLH_{-2}. Another open chain hexadentate

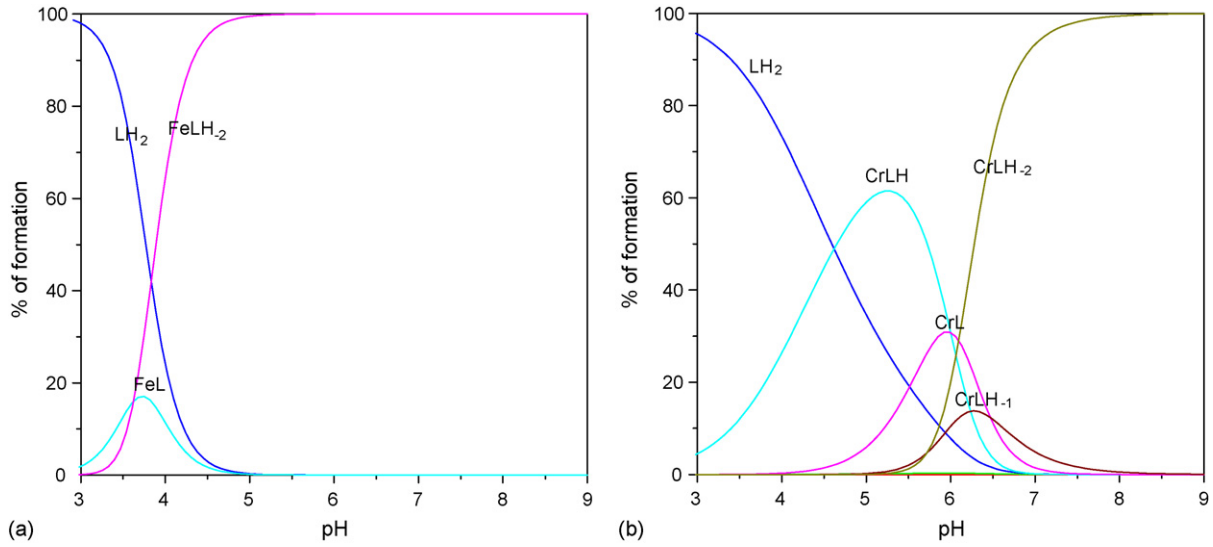

Fig. 10. Species distribution curves for 1:1 metal to ligand molar ratio for (a) the Fe-BHAEM and (b) Cr-BHAEM systems at $\mu = 0.1$ M $NaClO_4$ and $25 \pm 1\,^{\circ}C$ in aqueous medium.

(N,N,O) Schiff base ligand derived from salicylaldehyde and *N*,*N*′-bis(2,2′-aminoethyl)ethylenediamine (saltrien), which is structurally similar to BHAEM, acts as a hexadentate ligand towards a variety of metal complexes, and prefers a distorted octahedral arrangement about the metal ion, where the two oxygen atoms occupy *cis* positions and four nitrogen atoms (two *cis* amine and two *trans* imine groups) complete the coordination sphere [67], as shown by **D** or **E** in the present discussion.

3.5. Molecular modeling of metal complexes

In order to predict the structures of ML and MLH_{-2}, molecular modeling studies were undertaken. Both molecular mechanics (MM) and semi-empirical calculation were employed. Molecular mechanics calculates the steric energy, which partition into stretching, bending, torsion and nonbonded (e.g., Van der Waals, electrostatics, hydrogen bonding) interactions for the molecules and gives a stable structure with least strain energy. Although, the electronic properties cannot be predicted by molecular mechanics calculation, it still provides a computationally efficient tool to evaluate the degree to which a ligand is structurally organized for metal complexation and is useful for conformational analyses to obtain the stable conformers of the ligand both in the uncomplexed state and in its metal complexes. So, knowing the possible modes of coordination of a multidentate ligand for a metal ion and possible geometries for the metal complexes, MM models provide a way to quantify the effect of (a) cavity size, (b) different strain (bonded, nonbonded and angular), and (c) orientation of the donor groups in the metal complexes [68]. The computational strategy in this

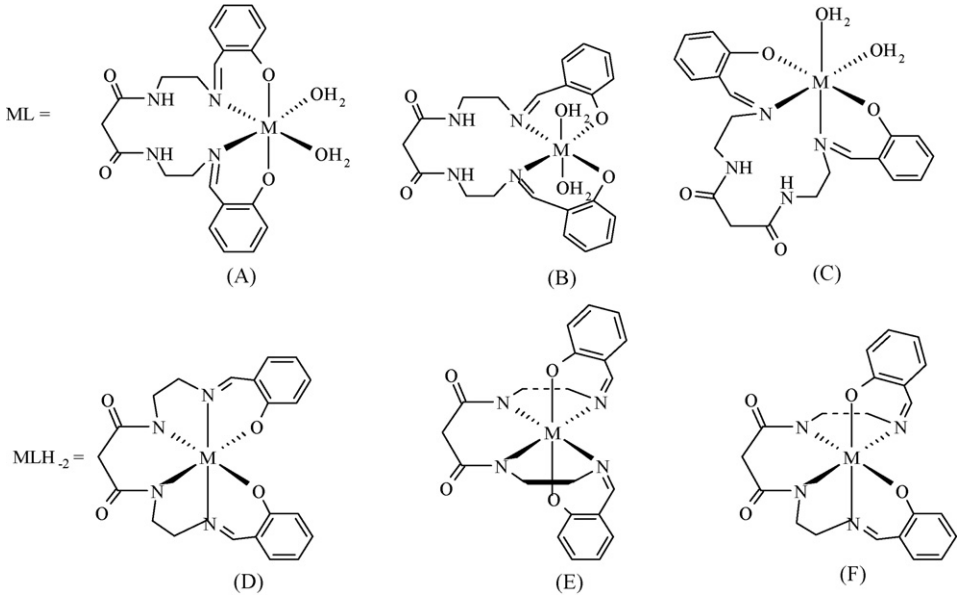

Fig. 11. Proposed possible coordination modes of BHAEM in solution.

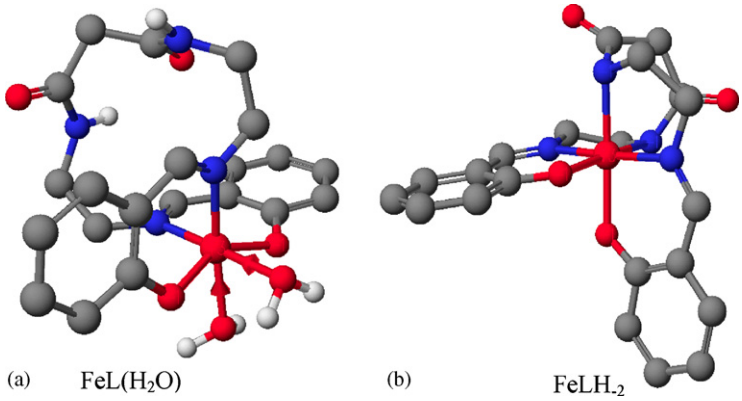

Fig. 12. The calculated structure of $FeL(H_2O)_2$ and $FeLH_{-2}$ using the semi-empirical AM1/d method (hydrogens are omitted for clarity).

study was to determine the minimum strain energy for various possible metal complex structures (Fig. 11). Molecular mechanics calculations were carried out using the MM3 force field to optimize the gas phase geometries of the complexes. We have also optimized the possible structures in which the dioxo groups participate in bond formation, but the strain energy was found to be higher compared with the structures shown in Fig. 11. The calculated strain energy of the different structures are given in Table 3.

The important results that emerge from Table 3, based on steric energy, is that in the $ML(H_2O)_2$ complex, the metal ion favours coordination through two *N*-amine and two *O*-phenolate groups. It was observed from the calculated strain energy that *cis*-$ML(H_2O)_2$ (**A** and **C**) forms show less strain than the corresponding *trans*-$ML(H_2O)_2$ (**B**) forms and among all $ML(H_2O)_2$ species, the most stable structure was **A**, coordinates through *2N*-amine and *2O*-phenolate groups with two water molecules at *cis* position. Among the three possible hexa-coordinated structures for MLH_{-2} species (**D**, **E** and **F**), structure **D** was found to be energetically more favorable than the configurations **E** and **F** for both metal ions, where two oxygen atoms occupy the *cis* position forming a distorted octahedral arrangement about the metal ion. This structure can also be attributed from the model structures. The strain imposed by the lack of free rotation of the C=N bond leads to the structure in which coordination of two phenolate groups from the same side results in minimum strain.

The semi-empirical AM1/d method has been employed to refine the probable structure of the Fe(BHAEM) complex. The strain free structures **A** and **D** for Fe(III) obtained through use of the MM3 method were re-optimized by applying the AM1/*d* Hamiltonian and the electronic spectrum was calculated from the optimized geometry using the semi-empirical ZINDO method. The optimized structures as shown in Fig. 12 shows a distorted octahedral geometry. Structurally, the geometry of **A** is more distorted than that of **D**. Some important calculated bond lengths for $FeLH_{-2}$ are Fe–N_{imine}, 2.055 Å; Fe–N_{amide}, 2.036 Å and Fe–O, 1.959 Å whereas bond angles (in °) are: N_{amide}–Fe–N_{amide}, 85.67; N_{imine}–Fe–N_{imine}, 177.34; N_{imine}–Fe–O, 88.13 and O–Fe–O, 84.88. The model structure indicates that the deprotonated amide nitrogen atom on coordination leads to a shortening of the bond length relative to coordination of the corresponding imine nitrogen atom. Such behaviour is well-documented for the coordination of other amide based ligands [48–52]. The calculated theoretical electronic spectra of FeL and $FeLH_{-2}$ along with that of the free ligand are shown in Fig. 13. A clear bathochromic shift is observed in the ligand peaks upon complexation, which corroborates well with the experimental results (Fig. 9). It has been suggested earlier that if the spectroscopic simulation, based on the energy-minimized structure is similar to the corresponding experimental data, then the calculated structure is likely to represent the global energy minimum of the compound for the environment where the spectroscopic data were collected [69].

Table 3
Calculated least strain energy (kcal/mol) structures for [M(BHAEM)]

Conformers	ML		Conformers	MLH_{-2}	
	Fe(III)	Cr(III)		Fe(III)	Cr(III)
A	−395.59	−392.08	**D**	−270.27	−268.25
B	−383.43	−380.28	**E**	−259.50	−256.25
C	−372.32	−366.71	**F**	−262.36	−260.26

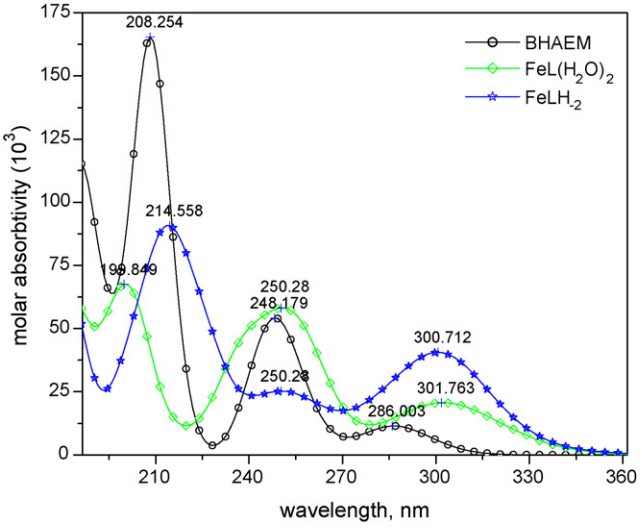

Fig. 13. Calculated electronic spectrum of BHAEM, $FeL(H_2O)_2$ and $FeLH_{-2}$ using the semi-empirical AM1/ZINDO method.

From the above evidence it may be inferred that the coordination of BHAEM with both Fe(III) and Cr(III) occurs first through two tertiary imine groups followed by two phenolate groups to give ML species, where two coordination sites are occupied by water molecules in *cis*-positions. As the pH increases, both complexes deprotonate and coordinate through the two amide groups to the metal ion to form the MLH_{-2} species.

4. Conclusion

By using a fluorescent method together with semi-empirical MO calculations, the existence of an excited state intramolecular proton transfer process has been established and a two step mechanism (dienol → enol-keto → diketo) rather than a one-step mechanism (dienol → diketo) was proposed. For trivalent iron and chromium ions, BHAEM coordinate in a tetradentate fashion under moderately acidic conditions, whereas under weakly acidic and basic conditions, it behaves as hexadentate ligand coordinating the respective metal ions through two imine nitrogens, two phenolate oxygens and two deprotonated amide nitrogen donors. The complexes of Fe(III) showed higher stability than that of Cr(III). The molecular modeling studies predicted a distorted octahedral geometry for both the ML and MLH_{-2} complexes as expected, the metal–amide nitrogen bond lengths in $FeLH_{-2}$ are shorter than the corresponding metal-imine nitrogen lengths.

References

[1] B. Witkop, L.K. Ramachandran, Metabolism 13 (1964) 1016.
[2] R.A. Morton, G.A.J. Pitt, Biochem. J. 59 (1955) 128.
[3] E. Grazi, R.T. Rowley, T. Cheng, O. Tchola, B.L. Horecker, Biochem. Biophys. Res. Commun. 9 (1962) 38.
[4] I. Fridovitch, F.H. Westheimer, J. Am. Chem. Soc. 84 (1962) 3208.
[5] G.G. Hammes, P. Fasella, J. Am. Chem. Soc. 84 (1962) 4644.
[6] B.S. Tovrog, D.J. Kitko, R.S. Drago, J. Am. Chem. Soc. 98 (1976) 5144.
[7] F. Lloret, M. Julve, M. Mollar, I. Castro, J. Latorre, J. Faus, X. Solans, I. Morgenstern-Badaran, J. Chem. Soc., Dalton Trans. (1989) 729.
[8] M. Calligaris, G. Manzini, G. Nardin, L. Randaccio, J. Chem. Soc., Dalton Trans. (1972) 5430.
[9] D. Cummins, E.D. McKenzie, H. Milburn, J. Chem. Soc., Dalton Trans. (1976) 130.
[10] N.A. Bailey, B.M. Higson, E.D. Mckenzie, J. Chem. Soc., Dalton Trans. (1972) 503.
[11] S.L. Kessel, R.M. Emberson, P.G. Debrunner, D.N. Hendrickson, Inorg. Chem. 19 (1980) 1170.
[12] A.M. Mahindra, J.M. Fisher, M. Rabinovitz, Nat. (Lond.) 303 (1983) 64.
[13] P.R. Palet, B.T. Thaker, S. Zele, Indian J. Chem. A38 (1999) 563.
[14] (a) C.M. Metzler, A. Cahill, D.E. Metzler, J. Am. Chem. Soc. 102 (1980) 6075;
(b) R.G. Fish, P.W. Groundwater, J.J.G. Morgan, Tetrahedron Asymmetry 6 (1995) 873;
(c) P. Przybylski, B. Brzezinski, Biopolym. Biospectrosc. 67 (2002) 61;
(d) P. Przybylski, K. Jasiński, B. Brzezinski, F. Bartl, J. Mol. Struct. 611 (2002) 193;
(e) P. Przybylski, B. Brzezinski, F. Bartl, Biopolym. Biospectrosc. 65 (2002) 111.
[15] A. Filarowski, A. Koll, Vib. Spectrosc. 17 (1998) 123.
[16] A. Koll, M. Rospenk, E. Jagodzinska, T. Dziembowska, J. Mol. Struct. 552 (2000) 193.
[17] S.H. Alarcon, D. Pagani, J. Bacigalupo, A.C. Olivieri, J. Mol. Struct. 475 (1999) 233.
[18] (a) F.L. Carter (Ed.), Molecular Electronic Devices II, Marcel Decker, New York, 1987;
(b) H. Durr, H. Bouas-Laurenet (Eds.), Photochromism: Molecules and Systems, Elsevier, Amsterdam, 1990;
(c) I. Willner, S. Rubin, Angew. Chem. Int. Ed. Engl. 35 (1996) 367.
[19] D.B. O'Connor, G.B. Scott, D.R. Coulter, A. Yavrouln, J. Phys. Chem. 95 (1991) 10252.
[20] T. Nishyiya, S. Yamuchi, N. Hirota, M. Baba, I. Hamazaki, J. Phys. Chem. 90 (1986) 5730.
[21] P.T. Chou, M.L. Martinej, Radiat. Phys. Chem. 41 (1993) 373.
[22] L.A. Hauch, C.L. Renschlar, Nucl. Instrum. Methods A 235 (1985) 41.
[23] A. Syntnik, J.C. Devella, J. Phys. Chem. 99 (1995) 13208.
[24] S.K. Das, S.K. Dogra, J. Colloid Int. Sci. 205 (1998) 443.
[25] M.D. Cohen, G.M. Schmidt, S.J. Flavian, J. Chem. Soc. (1964) 2041.
[26] P.F. Barbara, P.M. Rentzepis, L.E. Brus, J. Am. Chem. Soc. 102 (1980) 2786.
[27] D. Higelin, H. Sixl, Chem. Phys. 77 (1983) 391.
[28] W. Turbeville, P.K. Dutta, J. Phys. Chem. 94 (1990) 4060.
[29] M.Z. Zgierski, A. Grabowska, J. Chem. Phys. 112 (2000) 6329.
[30] (a) E.L. Roberts, J. Dey, I.M. Warner, J. Phys. Chem. A 100 (1996) 19681;
(b) E.L. Roberts, J. Dey, I.M. Warner, J. Phys. Chem. A 101 (1997) 5296.
[31] S.J. Formosinho, L.G. Arnaut, J. Photochem. Photobiol. A 75 (1993) 21.
[32] J. Dey, S.K. Dogra, J. Photochem. Photobiol. A 66 (1992) 15.
[33] T. Elsaesser, B. Schmetzer, Chem. Phys. Lett. 140 (1987) 293.
[34] C.A.S. Potter, R.G. Brown, Chem. Phys. Lett. 153 (1988) 7.
[35] R.S. Becker, C. Lenoble, A. Zein, J. Phys. Chem. 91 (1987) 3517.
[36] M. Bräuer, M. Masquera, J.L. Perez-Lustres, F. Rodriguez Prieto, J. Phys. Chem. A 102 (1998) 10736.
[37] M. Fores, M. Duran, M. Sola, L. Adamowicz, J. Phys. Chem. A 103 (1999) 4413.
[38] S. Nagaoka, A. Itoh, K. Mukai, U. Nagashima, J. Phys. Chem. 97 (1993) 11385.
[39] (a) N. Hoshino, T. Inabe, T. Mitani, Y. Maruyama, Bull. Soc. Chem. Jpn. 61 (1988) 4207;
(b) T. Inabe, N. Hoshino, T. Mitani, Y. Maruyama, Bull. Soc. Chem. Jpn. 62 (1989) 2245;
(c) T. Inabe, New J. Chem. 15 (1991) 129;
(d) S. Takeda, H. Chihara, T. Inabe, T. Mitani, Y. Maruyama, Chem. Phys. Lett. 189 (1992) 13;
(e) S. Takeda, T. Inabe, C. Benedict, U. Langer, H.H. Limbach, Ber. Bunsenges. Phys. Chem. 102 (1998) 1358.
[40] M.Z. Zgierski, A. Grabowska, J. Chem. Phys. 113 (2000) 7845.
[41] A. Grabowska, K. Kownacki, L. Kaczmarck, Acta Phys. Pol. A 88 (1995) 1081.
[42] L.Z. Zhang, G.Q. Tang, J. Fluorescence 15 (2005) 13.
[43] (a) F. Lloret, J. Moratal, J. Faus, J. Chem. Soc., Dalton Trans. (1983) 1749;
(b) F. Lloret, J. Moratal, J. Faus, J. Chem. Soc., Dalton Trans (1983) 1743.
[44] (a) R.H. Molina, A. Mederos, P. Gili, S. Dominguez, P. Nunez, Polyhedron 16 (1997) 4191;
(b) R.H. Molina, A. Mederos, P. Gili, S. Dominguez, P. Nunez, G. Germain, T. Debaerdemaeker, Inorg. Chim. Acta 256 (1997) 319.
[45] (a) R.J. Motekaitis, A.E. Martell, Inorg. Chem. 27 (1988) 2718;
(b) R.J. Motekaitis, A.E. Martell, D.A. Nelson, Inorg. Chem. 23 (1984) 275.
[46] (a) D.F. Evans, D.A. Jakubovic, J. Chem. Soc., Dalton Trans (1988) 2927;
(b) D.F. Evans, D.A. Jakubovic, Polyhedron 7 (1988) 1881;
(c) D.F. Evans, P.H. Missen, J. Chem. Soc., Dalton Trans (1987) 1279.
[47] S.K. Sahoo, S.E. Muthu, M. Baral, B.K. Kanungo, Spectrochim. Acta A 63 (2006) 574.
[48] J.D. Bell, H.C. Freeman, A.M. Wood, R. Driver, W.R. Walker, J. Chem. Soc., Chem. Commun. (1969) 1441.
[49] (a) M. Kodama, E. Kimura, J. Chem. Soc., Dalton Trans. (1981) 694;
(b) M. Kodama, T. Koike, E. Kimura, Bull. Chem. Soc. Jpn. 68 (1995) 1627.
[50] M. Di Casa, L. Fabrizzi, A. Perotti, A. Poggi, P. Tundo, Inorg. Chem. 24 (1985) 1610.
[51] T. Toki, M. Mikuriya, H. Okawa, I. Murase, S. Kida, Bull. Chem. Soc. Jpn. 57 (1984) 2098.

[52] S. Zhu, F. Kou, H. Lin, C. Lin, M. Lin, Y. Chen, Inorg. Chem. 35 (1996) 5851.
[53] (a) V. Amendola, L. Fabrizzi, C. Mangano, P. Pallavicini, A. Perotti, A. Taglietti, J. Chem. Soc., Dalton Trans. (2000) 185;
(b) V. Amendola, C. Brusoni, L. Fabrizzi, C. Mangano, H. Miller, P. Pallavicini, A. Perotti, A. Taglietti, J. Chem. Soc., Dalton Trans. (2001) 3528.
[54] L. Fabrizzi, M. Licchelli, P. Pallavicini, A. Perotti, D. Sacchi, Angew. Chem. Int. Ed. Engl. 33 (1994) 1975.
[55] A.E. Martell, R.J. Motekaitis, The Determination and Use of Stability Constants, VCH Publishers, New York, 1992.
[56] H. Gampp, M. Maeder, C.J. Meyer, A.D. Zuberbuhler, Talanta 32 (1985) 95.
[57] P. Gans, A. Sabatini, A. Vacca, Ann. Chim. 89 (1999) 45.
[58] Computational Chemistry Manual for HyperChem version 7.5, Hypercube Inc., 419 Philip Street, Waterloo, Ontario, Canada N2L 3X2, 2003.
[59] C. Peng, H.B. Schlegel, Israel J. Chem. 33 (1993) 449.
[60] User Guide Manual for CAChe version 6.01, Fujitsu Limited, 2003.
[61] S. Ressalan, C.S.P. Iyer, J. Luminesc. 111 (2005) 121.
[62] P.B. Bisht, H.B. Tripathi, D.D. Pant, J. Photochem. Photobiol. A 103 (1995) 5290.
[63] M.S. Dewar, E.G. Zoebisch, E.F. Healy, J.P. Stewart, J. Am. Chem. Soc. 107 (1985) 3902.
[64] F.A. Cotton, G. Wilkinson, C.A. Murillo, M. Bochmann, Advanced Inorganic Chemistry, sixth ed., John Wiley & Sons, Inc., Singapore, 1999.
[65] M. Calligaris, G. Nardin, L. Randaccio, Coord. Chem. Rev. 7 (1972) 385.
[66] (a) T.J. Collins, R.D. Powell, C. Slebodnick, E.S. Uffelman, J. Am. Chem. Soc. 113 (1991) 8419;
(b) D.W. Margerum, Pure Appl. Chem. 55 (1983) 23.
[67] (a) P.D. Cradwick, M.E. Cradwick, G.G. Dodson, D. Hall, T.N. Waters, Acta Crystallogr., Sect. B 28 (1972) 45;
(b) E. Sinn, G. Sinn, E.V. Dose, M.F. Tweedle, L.J. Wilson, J. Am. Chem. Soc. 100 (1978) 3375.
[68] P. Comba, T.W. Hambley, Molecular Modeling of Inorganic Chemistry, VCH Publishers, Inc., New York, 1995.
[69] P. Comba, Comm. Inorg. Chem. 16 (1994) 133.